Published online 6 January 2016 *Nucleic Acids Research, 2016, Vol. 44, No. 5* **2199–2213**
doi: 10.1093/nar/gkv1523

S. cerevisiae Mre11 recruits conjugated SUMO moieties to facilitate the assembly and function of the Mre11-Rad50-Xrs2 complex

Yu-Jie Chen[1,2,3,4], Yu-Chien Chuang[4], Chi-Ning Chuang[4], Yun-Hsin Cheng[4], Chuang-Rung Chang[1,2], Chih-Hsiang Leng[1,3,*] and Ting-Fang Wang[4,*]

[1]Graduate Program of Biotechnology in Medicine, National Tsing Hua University and National Health Research Institutes, Taiwan, [2]Institute of Biotechnology, National Tsing Hua University, Hsinchu 300, Taiwan, [3]National Institute of Infectious Diseases and Vaccinology, National Health Research Institute, Miaoli 350, Taiwan and [4]Institute of Molecular Biology, Academia Sinica, Taipei 115, Taiwan

Received February 24, 2015; Revised December 01, 2015; Accepted December 19, 2015

ABSTRACT

Double-strand breaks (DSBs) in chromosomes are the most challenging type of DNA damage. The yeast and mammalian Mre11-Rad50-Xrs2/Nbs1 (MRX/N)-Sae2/Ctp1 complex catalyzes the resection of DSBs induced by secondary structures, chemical adducts or covalently-attached proteins. MRX/N also initiates two parallel DNA damage responses—checkpoint phosphorylation and global SUMOylation—to boost a cell's ability to repair DSBs. However, the molecular mechanism of this SUMO-mediated response is not completely known. In this study, we report that *Saccharomyces cerevisiae* Mre11 can non-covalently recruit the conjugated SUMO moieties, particularly the poly-SUMO chain. Mre11 has two evolutionarily-conserved SUMO-interacting motifs, Mre11^{SIM1} and Mre11^{SIM2}, which reside on the outermost surface of Mre11. Mre11^{SIM1} is indispensable for MRX assembly. Mre11^{SIM2} non-covalently links MRX with the SUMO enzymes (E2/Ubc9 and E3/Siz2) to promote global SUMOylation of DNA repair proteins. Mre11^{SIM2} acts independently of checkpoint phosphorylation. During meiosis, the *mre11^{SIM2}* mutant, as for *mre11S*, *rad50S* and *sae2*Δ, allows initiation but not processing of Spo11-induced DSBs. Using MRX and DSB repair as a model, our work reveals a general principle in which the conjugated SUMO moieties non-covalently facilitate the assembly and functions of multi-subunit protein complexes.

INTRODUCTION

Small ubiquitin-like modifier (SUMO) is a small regulatory protein found in almost all eukaryotic organisms (1–3). In the yeast *Saccharomyces cerevisiae*, the essential gene *SMT3* encodes the SUMO protein. SUMOylation is a post-translational modification, in which SUMO is covalently attached to a substrate protein including SUMO itself, to form a poly-SUMO chain. SUMOylation is mediated by an enzymatic cascade that is analogous to the one that is involved in ubiquitination. The removal of the SUMO adduct from targets is catalyzed by specific SUMO proteases, e.g. Ulp1 and Ulp2. The conjugated SUMO moieties (CSMs) are recognized by two types of SUMO-binding motifs, short hydrophobic sequences known as SUMO-interacting motifs (SIMs) (4) and the ZZ zinc fingers (5,6). The addition, removal and recognition of SUMO are influenced by and affect a plethora of cellular pathways. Because SUMOylation frequently targets entire groups of physically interacting proteins rather than individual proteins, it has been proposed that protein-group SUMOylation functions to establish new physical interactions between proteins that have SUMO-binding motifs (7). Alternatively, CSMs can covalently or non-covalently prevent premature aggregation by increasing the water solubility of individual protein subunits (8,9) prior to their assembly into a functional protein complex (10–12). A proof-of-concept has been provided by simultaneously expressing three capsid proteins of the foot-and-mouth disease virus (FMDV); these three SUMO fusion proteins formed a stable heterotrimeric complex. The proteolytic removal of SUMO moieties from the ternary complexes resulted in virus-like particles with a size and shape resembling the authentic FMDV, which contains 20 heterotrimers of the capsid proteins (10).

SUMOylation is strongly connected to the repair of DNA double-strand breaks (DSBs) (13). In *S. cerevisiae* vege-

*To whom correspondence should be addressed. Tel: +886 2 27899188; Fax: +886 2 27826508; Email: tfwang@gate.sinica.edu.tw
Correspondence may also be addressed to Chih-Hsiang Leng. Tel: +886 37 246166 ext 37711; Fax: +886 37 583009; Email: leoleng@nhri.org.tw

tative cells, mutations or deletion of SUMOylation genes cause a pronounced sensitivity to DNA damage and genomic instability, including the poly-SUMO chain mutant (*smt3-allR*) (14), E2 conjugating enzyme (*ubc9*), E3 ligase enzymes (*siz1*Δ, *siz2*Δ, *mms21*) (7,15), deSUMOylation proteases ($ulp1^{ts}$, *ulp2*Δ) (16,17) as well as SUMO-targeted ubiquitin ligases (STUbLs; *slx5*Δ, *slx8*Δ) (18,19). In parallel, with checkpoint phosphorylation, vegetative yeast cells also induce SUMOylation of many proteins that are needed for replication and repair in response to DNA damage (7,15). The MRX (Mre11-Rad50-Xrs2)-Sae2/Com1 dsDNA endonuclease complex has been implicated as a positive regulator for DSB-induced global SUMOylation (15). Mre11 exhibits notable two-hybrid interactions with Ubc9 and Siz2, and it has been proposed that the binding of Siz2 might be achieved through Ubc9-catalyzed SUMOylation of Mre11 (7). Sae2 (also called Com1)(20) is a SUMOylated protein during vegetative growth, and SUMOylation of Sae2 increases both soluble Sae2 and the MRX function in DNA end resection (21). Sae2 apparently mediates removal of the MRX complex from the DNA damaged sites during vegetative growth. The MRX complex is retained at DSB ends in *sae2*Δ, thus turning on the DNA damage checkpoint to stall cell cycle progression (22,23). Recently, it has been reported that, following the resection of DSBs, Siz2 also collaborates with the ssDNA binding complex RPA (replication protein A) to enhance global SUMOylation (7,24). The relationship between MRX and RPA in promoting DSB-induced SUMOylation and the molecular mechanism of the interaction between MRX and Sae2 interactions remains unclear.

MRX has multiple functions during *S. cerevisiae* meiosis (25,26). First, it has a unique role in Spo11-induced DSBs independently of its catalytic activity, and the C-terminal portion of Mre11 is specifically required for this function (27,28). Second, the MRX-Sae2 endonuclease complex acts at each 5′-end of DSBs to generate 3′-end ssDNA tails through the removal of a covalently linked Spo11-oligonucleotide complex (29,30). The 3′-end ssDNA tails subsequently assemble into nucleoprotein filaments comprised of two RecA-family recombinases (Rad51 and Dmc1) and their accessory factors to catalyze DSB repair via homologous recombination (31–33). Third, MRX senses DSBs and activates the $Tel1^{ATM}$ checkpoint kinase for target phosphorylation. This checkpoint phosphorylation has dual roles in preventing superfluous Spo11-induced DSBs (34,35) and in promoting interhomolog recombination (12,35,36). Interhomolog recombination is a hallmark of meiotic recombination. A few Spo11-induced DSBs must be repaired using a homologous non-sister chromosome (but not a sister chromatin) as template to generate new combinations of DNA sequences (26).

Accumulating evidence has also revealed that SUMOylation functionally links two groups of *S. cerevisiae* proteins that are essential for interhomolog recombination. The first group includes three meiosis-specific chromosomal proteins Hop1, Red1 and Mek1. These proteins are the axial components of the synaptonemal complex (SC)—a zipper-like proteinaceous structure that mediates chromosome synapsis between homologous chromosomes during meiotic prophase. The SC consists of two dense lateral/axial elements and a central element. To assemble the SC, both the SC central protein, Zip1, and the SC axial protein, Red1, non-covalently interact with conjugated SUMO moieties (CSMs), such as poly-SUMO chains or conjugates. During SC assembly, the SC initiation protein, Zip3, acts as a SUMO E3 ligase that promotes the formation of additional CSMs (11,37). Consistent with these findings, it has been shown that the SUMOylation of Ubc9 promotes the formation of a poly-SUMO chain, which is a key event for SC formation (38). Furthermore, SUMOylation and the ubiquitin-mediated removal of CSMs (e.g. SUMOylated topoisomerase II or Red1) have been implicated in SC-mediated crossover interference (39). Crossover interference is a genetic phenomenon in which crossovers tend to be evenly spaced along any given meiotic chromosomes. SUMOylation is also critical in the regulation of meiotic recombination or chromosomal morphogenesis in other sexually-reproductive organisms, including the fission yeast *S. pombe* (40), the fungus *Sordaria* (41), *Arabidopsis thaliana* (42) and mammals (43).

The DNA damage checkpoint proteins $Mec1^{ATR}$ and $Tel1^{ATM}$ are the second group required for establishing interhomolog bias during meiotic recombination. $Tel1^{ATM}$ is activated by non-resected DSBs via an Xrs2-dependent mechanism (44–47), and $Mec1^{ATR}$ is recruited to RPA-coated ssDNA tails via its binding partner, Ddc2 (48,49). $Mec1^{ATR}$ activation also requires three additional DNA damage sensors: the yeast 9-1-1 complex (Ddc1-Mec3-Rad17), its clamp loader, the Rad24-RFC complex and Dpb11 (48,50–52). These two protein kinases phosphorylate the SC axial protein Hop1 to ensure interhomolog recombination (11,12,36,53,54). Notably, both $Tel1^{ATM}$- and $Mec1^{ATR}$-dependent Hop1 phosphorylation requires Red1 and the Red1-CSM interaction (11,36). Red1 first non-covalently associates with CSMs (11) and then with the 9-1-1 complex (55) to activate $Mec1^{ATR}$ resulting in Hop1 phosphorylation via its binding to the 9-1-1 complex (12). It is still unclear how the Red1-CSM ensemble couples with MRX at the non-resected DSB ends during meiosis.

Here, we investigate the molecular mechanism and physiological impacts of the Mre11-SUMO interaction in response to DSBs during vegetative growth and meiosis. Our results reveal that the yeast *S. cerevisiae* Mre11 can non-covalently recruit CSMs to facilitate both global SUMOylation and DSB repair.

MATERIALS AND METHODS

Yeast strains, two-hybrid assay and physical analysis

All vegetative experiments were performed using haploid cells from isogenic W303 strains as described previously (15,56). All meiotic experiments were performed using diploid cells from isogenic SK1 strains. Quantitative yeast two-hybrid assays, tetrad dissection, fluorescence-activated cell sorting (FACS), pulsed-field gel electrophoresis (PFGE) and Southern hybridization were carried out as previously described (11,36,37).

Antisera, immunoblot, dephosphorylation assay and cytology

The antisera used against Hop1, phosphorylated Hop1-T318, Zip1, phosphorylated Zip1-S75, H2A and phosphorylated H2A-S129 have been described previously (36). Peroxidase-anti-peroxidase (PAP) antibody (Sigma, CA, USA), IgG Sepharose beads (GE Healthcare, Bucks, UK), anti-HA antibody (Roche, Basel, SWZ) and anti-Rad53 antibody (Santa Cruz Biotechnology, TX, USA) were purchased commercially. Western blotting analyses were performed as recently described and repeated 2-4 times (36). The dephosphorylation assay was performed as described previously (54). Cytology analyses were carried out as previously described (11,37).

Immunoprecipitation

Yeast vegetative cultures (20 ml; OD_{600} ≈0.5) were harvested and washed once with ice-cold water. Cells were resuspended in 250 μl of lysis buffer (50 mM Tris-HCl pH 7.5, 150 mM NaCl, 5 mM EDTA pH 8.0, 0.1% Triton X-100) containing an EDTA-free protease inhibitor complete cocktail (Roche) and 20 mM N-ethylmaleimide (Sigma). To prepare the total cell lysates, the cell suspension was mixed with 1/2 volume of 0.5-mm acid-washed glass beads (Sigma), vigorously vortexed (30 s of vortexing and 30 s on ice) five times, and then microcentrifuged (16 000 x g) at 4°C for 10 min. The supernatants were collected and incubated with IgG Sepharose beads (Sigma) or immobilized anti-HA affinity resin (Sigma) at 4°C for 2 h. The precipitants were washed three times with 1 ml of lysis buffer and then resuspended in 100 μl Laemmli loading buffer containing 100 mM dithiothreitol. The proteins were analyzed by SDS-PAGE and immunoblotting as described previously (11).

RESULTS

Identification of two SUMO-interacting motifs (SIMs) in Mre11 that preferentially interacts with the poly-SUMO chain

We identified, *in silico*, two putative SIMs in *S. cerevisiae* Mre11: $Mre11^{SIM1}$ (IRIL, residues 9-12) and $Mre11^{SIM2}$ (ESDKIKVV, residues 154-161) (57). Both SIMs are evolutionarily conserved in *S. pombe* Mre11: $Mre11^{SIM1}$ (IRIL, residues 18-21) and $Mre11^{SIM2}$ (ENDNIVV, residues 163-169) (Figure 1A). Furthermore, they reside at the outermost surface of the *S. pombe* Mre11-Nbs1 complex crystal structure (58) (Figure 1A). Nbs1 is the *S. pombe* homolog of Xrs2. Thus, Mre11 might non-covalently associate with the SUMO monomer or CSMs.

These two distinct possibilities were further examined by two-hybrid assays with either vegetative or meiotic two-hybrid reporter cells (11,59). We found that Mre11 preferentially interacts with CSMs rather than the Smt3 monomer; the hierarchy for two-hybrid interactions with Mre11 was Smt3 > Smt3-allR > Smt3-ΔGG ≅ mock control in both vegetative and meiotic reporter cells (Table 1). Smt3-allR cannot form a polymeric chain because the nine lysine residues in the wild type Smt3 are replaced by arginine, but it remains competent in the SUMO conjugation with all target proteins (including wild-type Smt3) (60). Smt3-ΔGG is a conjugation-incompetent Smt3 mutant that lacks the C-terminal pair of glycines required for E1-mediated Smt3 activation (61). Next, we constructed two SIM mutant proteins ($Mre11^{I9R}$ and $Mre11^{I158R}$), each with a mutation from isoleucine (I) to arginine (R). We found that neither of these two mutants exhibited notable two-hybrid interactions with Smt3, Smt3-allR or Smt3-ΔGG (Table 1).

S. cerevisiae Mre11 exhibits strong two-hybrid interactions with the SUMO E2 enzyme Ubc9 and the SUMO E3 ligase Siz2 (7), and Mre11 is also a SUMOylated protein (7,11). We examined whether the Mre11-Ubc9 and Mre11-Siz2 interactions are mediated via SUMOylated Mre11 or non-covalently via the Mre11-CSM ensembles. We found that the hierarchy for the two-hybrid interaction with Ubc9 or $Siz2_{348-726}$ was Mre11 > $Mre11^{I158R}$ ≅ $Mre11^{I9R}$ ≅ mock control (Table I). $Siz2_{348-726}$ is the C-terminal domain of Siz2 and harbors two SIMs (11). These results suggest that both interactions are likely mediated via the Mre11-CSM ensembles rather than SUMOylated Mre11 (also see below).

To minimize the potential effects of arginine replacement on protein structure or folding, we also constructed additional $Mre11^{SIM1}$ and $Mre11^{SIM2}$ mutants with one, two or three alanine mutations, respectively. All these mutants exhibited reduced or no two-hybrid interactions with Smt3, Smt3-allR or Smt3-ΔGG (Supplementary file, Supplementary Table S1). The hierarchy for the two-hybrid interaction of the $Mre11^{SIM1}$ mutants with Smt3 was Mre11 >> $Mre11^{I11A}$ > $Mre11^{I9A}$ > $Mre11^{I9A,I11A}$ ≅ $Mre11^{I9R}$, and that of the $Mre11^{SIM2}$ mutants with Smt3 was Mre11 >> $Mre11^{I158A}$ > $Mre11^{I158A,V161A}$ ≅ $Mre11^{V160A, V161A}$ ≅ $Mre11^{I158R}$ ≅ $Mre11^{V160A}$ > $Mre11^{V161A}$ ≅ $Mre11^{I158A,V160A}$.

$Mre11^{I9R}$ is defective in MRX assembly

Mre11 displays strong two-hybrid interactions with Xrs2 and Rad50 (62). Using both vegetative and meiotic two-hybrid reporter cells (11,59), we found that $Mre11^{I158R}$ (as for Mre11) exhibited notable two-hybrid interactions with Xrs2 and Rad50. In contrast, $Mre11^{I9R}$ failed to interact with Rad50 and Xrs2 in the same assay (Table 1).

Next, we constructed three W303 strains (*MRE11-6HA*, *mre11^{I9R}-6HA*, *mre11^{I158R}-6HA*) that express an HA-epitope-tagged wild-type and mutant Mre11, respectively. Compared to *MRE11-6HA* and *mre11^{I158R}-6HA*, the *mre11^{I9R}-6HA* mutant displayed a slow vegetative growth phenotype on the YPD plate (Figure 1B). The hierarchy for resistance to the DNA damage agent methyl methanesulfonate (MMS) is *MRE11* ≅ *MRE11-6HA* > *mre11^{I158R}-6HA* >> *mre11^{I9R}-6HA* ≅ *mre11*Δ (Figure 1B). Again, to minimize the potential effects of arginine replacements on protein structure or folding, we also expressed and compared different $Mre11^{SIM1}$-6HA and $Mre11^{SIM2}$-6HA mutants for MMS resistance in a SK1 *mre11*Δ mutant (Figure 1C). For all the mutants examined here, their two-hybrid interactions with Smt3 correlated well with the hierarchy for MMS resistance (Figure 1C): *MRE11-6HA* > *mre11^{I11A}-6HA* > *mre11^{I9A}-6HA* > *mre11^{I9A,I11A}-6HA* ≅ *mre11^{I9R}-6HA* ≅ *mre11*Δ and *MRE11-6HA* >> *mre11^{V160A}-6HA* ≅ *mre11^{V161A}-*

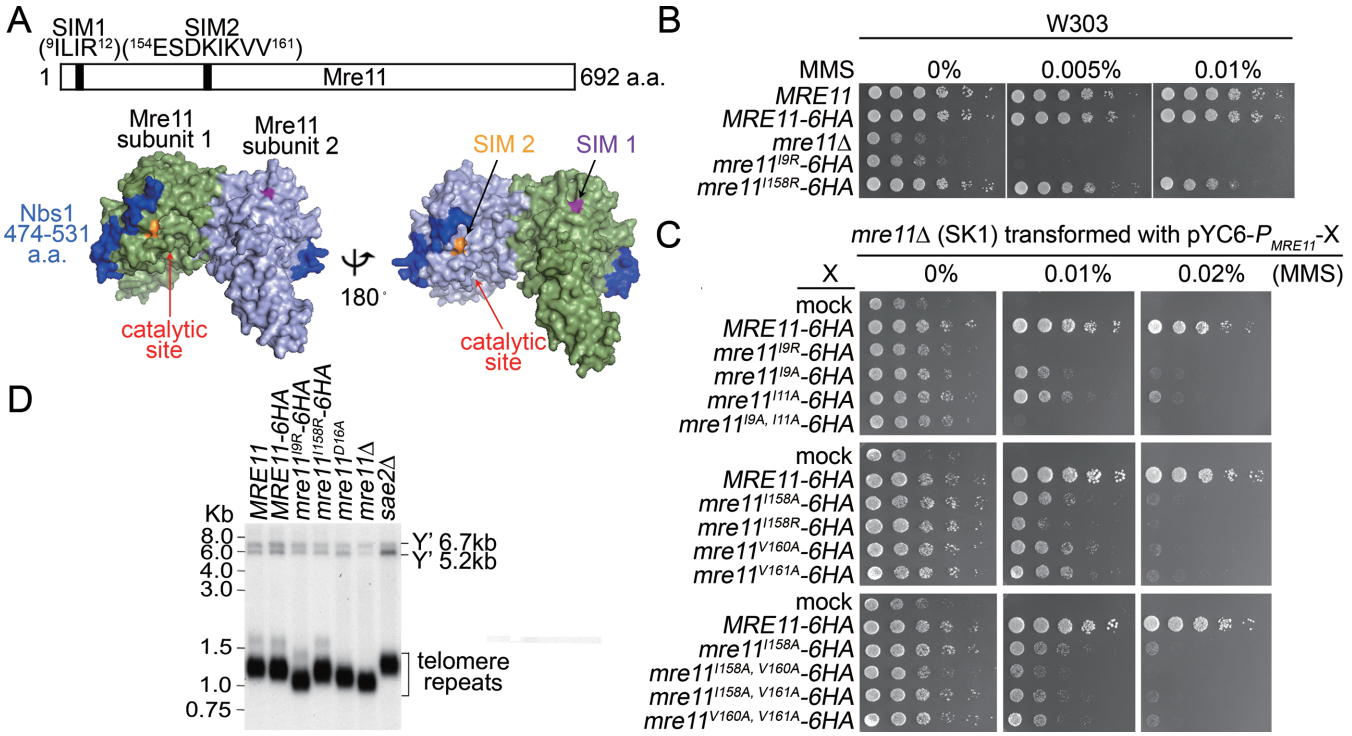

Figure 1. *S. cerevisiae* Mre11 protein has two SUMO-interacting motifs (SIMs) that are differentially required for MMS resistance and telomere length maintenance. (**A**) Schematic representation of full-length *S. cerevisiae* Mre11, Mre11^{SIM1} and Mre11^{SIM2}, and their amino acid sequences. Mre11^{SIM1} and Mre11^{SIM2} are evolutionarily conserved in *S. pombe* Mre11. Shown in the lower panel is the crystal structure of Nbs1 (474–531 amino acid residues; in blue) and the two full-length Mre11 subunits (in gray and dark green)(58). SIM1 and SIM2 are indicated in purple and orange, respectively. The catalytic site of *S. pombe* Mre11 is indicated by a red arrow. (**B, C**) Spot assay showing the five-fold serial dilutions of W303 (B) and (C) SK1 haploid strains grown on YPD plates and YPD plates containing MMS at the indicated concentrations. The SK1 *mre11*Δ haploid strains were transformed with an pYC6-P_{MRE11} vector for expressing various Mre11 proteins as indicated. P_{MRE11} is the promoter of the wild-type *MRE11* gene. (**D**) Telomere length. *Xho*I-digested genomic DNA was separated on a 1.2% agarose gel and Southern hybridized with a Y′ probe. The terminal telomere repeats form heterogeneous fragments of ≈1.3 kb, whereas the Y′ long and short subtelomeric repeat sequences appear at the top of the gel (56).

Table 1. Two-hybrid analyses[1]

Gal4AD-X	Host cell	X-Y interaction[1]					
		LexA-Y					
		Mre11	Mre11^{I9R}	Mre11^{I158R}	Mre11^{D16A}	Mre11^{P84S}	Mre11^{T188I}
mock	Vegetative growth	0.4 ± 0.1	0.3 ± 0.0	0.5 ± 0.3	1.2 ± 0.6	0.2 ± 0.0	0.2 ± 0.1
Smt3		71.9 ± 0.6	0.8 ± 0.0	7.6 ± 1.3	8.1 ± 5.5	51.7 ± 3.1	60.1 ± 3.6
Smt3^{allR}		21.8 ± 0.1	0.6 ± 0.0	1.9 ± 0.3	1.7 ± 2.0	11.2 ± 1.3	16.6 ± 2.8
Smt3$^{\Delta GG}$		0.7 ± 0.0	0.3 ± 0.0	0.2 ± 0.0	1.8 ± 0.6	0.2 ± 0.0	0.3 ± 0.0
Ubc9		63.6 ± 2.0	0.8 ± 0.4	2.4 ± 1.0	n.d.[2]	54.6 ± 1.7	48.3 ± 2.5
$Siz2_{348–726}$		79.8 ± 2.1	0.3 ± 0.2	7.8 ± 1.2	n.d.[2]	84.2 ± 6.2	41.4 ± 2.1
Rad50		135.2 ± 5.7	2.6 ± 0.1	106.0 ± 4.8	5.8 ± 2.9	121.1 ± 4.2	55.2 ± 4.9
Xrs2		188.1 ± 8.5	0.3 ± 0.0	37.9 ± 4.0	76.2 ± 7.0	161.9 ± 6.4	153.4 ± 4.7
mock	Meiosis[3] (*ndt80*Δ)	0.7 ± 0.3	0.6 ± 0.3	0.3 ± 0.1	n.d.[2]	n.d.[2]	n.d.[2]
Smt3		38.8 ± 5.8	0.6 ± 0.3	1.4 ± 0.3			
Smt3^{allR}		5.4 ± 1.9	0.9 ± 0.5	0.8 ± 0.2			
Smt3$^{\Delta GG}$		0.7 ± 0.3	0.7 ± 0.3	0.4 ± 0.1			
Rad50		54.7 ± 0.9	1.0 ±0.5	26.0 ± 1.0			
Xrs2		125.3 ± 9.5	0.6 ± 0.3	35.1 ± 1.0			

[1]The two-hybrid interaction was determined by measuring the β-galactosidase activity. One unit of β-galactosidase hydrolyzes 1 μmol of o-nitrophenyl β-galactopyranoside per min per OD_{600} (optical density at 600 nm) unit.
[2]n.d. (not determined).
[3]Meiotic two-hybrid analysis using an *ndt80*Δ diploid strain (11,59)

6HA > *mre11*^{V160A,V161A}*-6HA* ≅ *mre11*^{I158A,V161A}*-6HA* ≅ *mre11*^{I158A}*-6HA* > *mre11*^{I158A,V160A}*-6HA* ≅ *mre11*^{I158R}*-6HA* > *mre11*Δ.

The *S. cerevisiae* MRX is also required for telomere length maintenance. Like *mre11*Δ, *mre11*^{D16A} exhibits severe phenotypes in DNA repair and telomere maintenance. Mre11^{D16A} is defective in MRX assembly and lacks endonuclease activity (56). We first confirmed that Mre11^{D16A} exhibits defects in two-hybrid interactions with Smt3 and Rad50 but not Xrs2 (Table 1). Next, we showed that the hierarchy for telomere length maintenance was *MRE11* ≥ *MRE11-6HA* ≅ *sae2*Δ > *mre11*^{I158R}*-6HA* > *mre11*^{D16A} > *mre11*^{I9R}*-6HA* ≅ *mre11*Δ (Figure 1D). Genomic DNA was isolated from all strains, digested with *XhoI* and Southern hybridized for telomeric sequences. Consistent with previous reports, the telomeres in *mre11*Δ are shorter than those in *mre11*^{D16A} (56) and the *sae2*Δ deletion does not affect the maintenance of normal telomere length (63). These results indicate that *mre11*^{I9R} is phenotypically similar to *mre11*Δ, confirming that Mre11^{I9R} is defective in MRX assembly. In contrast, *mre11*^{I158R}*-6HA* showed much milder defects in MMS-resistance (Figure 1B,C) and telomere maintenance (Figure 1D). Thus, Mre11^{I158R} apparently can form a functional (at least partly) MRX complex.

D16 is one of seven essential and evolutionarily-conserved amino acid residues that coordinate two Mn^{2+} ions to form the phosphodiesterase active site (64). Because Mre11^{D16A} is defective in association with the Mn^{2+}, A16 and its neighboring amino acid residues (such as SIM1: IRIL, residues 9–12) might be improperly folded. As a result, Mre11^{D16A} is unable to interact with SUMO. Alternatively, D16 should be classified as being part of SIM1, or the SIM1-CSM interaction might mask D16 from chelating with Mn^{2+}. In this scenario, Mre11 first recruits CSMs to facilitate Mre11 folding and/or MRX assembly. After replacement of CSMs with Mn^{2+}, the folded Mre11 protein or the assembled MRX complex is no longer able to associate with CSMs via SIM1. This possibility is more logical, because it is consistent with the results of our two-hybrid (Table 1) and pull-down experiments (see below) showing neither Mre11^{I9R} nor Mre11^{I158R} is unable to interact with CSMs.

Mre11^{I9R} and Mre11^{I158R} are differentially defective in their ability to repair spontaneous and MMS-induced DNA damage

When DNA replication forks are stalled by spontaneous or MMS-induced DNA lesions, checkpoint proteins are activated to stabilize those stalled forks. Stalled forks eventually collapse and produce broken DSBs. The recovery of DNA replication is typically controlled by MRX-dependent repair of DSBs (65–67). Here, we compared the recovery of DNA replication in *MRE11-6HA*, *mre11*^{I9R}*-6HA* and *mre11*^{I158R}*-6HA* (Figure 2A). Cells were first arrested in G1 by mating pheromone α-factor and then released into S phase; this time point was referred to as T0. After 10 min, different amounts of MMS (0, 0.01%, 0.033%) were added to the cells for 45 min. This time point was referred to as T55, i.e. 55 min after release from α-factor arrest. Next, MMS was removed from the cells for 3 h (referred to as T235) to determine the recovery of DNA replication (Figure 2A). DNA replication was monitored by fluorescence-activated cell sorting (FACS; Figure 2B) and pulsed-field gel electrophoresis (PFGE; Figure 2C). Checkpoint activation was determined by Western blot analysis with anti-Rad53 antisera (Figure 2D). Rad53 is an essential DNA damage checkpoint protein kinase that is required for cell-cycle arrest in response to DNA damage. Rad53 activation occurs through direct phosphorylation by Mec1^{ATR} and Tel1^{ATM} followed by Rad53 autophosphorylation (68,69). The hyperphosphorylated Rad53 protein is distinguishable from the unphosphorylated Rad53 protein, as the latter migrates faster in a SDS-PAGE gel (68).

The steady-state levels of these three HA-tagged Mre11 proteins were not significantly different at T0, T55 or T235 (Figure 2D). To examine their protein stability, we performed cycloheximide shut-off experiments (Supplementary Figure S1A). Protein synthesis was inhibited by 200 μg/ml of cycloheximide added into the vegetative cultures. Samples were taken at 0, 30, 60, 90, 120 and 180 min after the addition of cycloheximide (Supplementary Figure S1A, lower panel). The immunoblotting results revealed that Mre11-6HA, Mre11^{I9R}-6HA and Mre11^{I158R}-6HA exhibited similar half-lives ($t_{1/2}$ ≈45-60 min) in the presence of cycloheximide up to 180 min (Supplementary Figure S1C), suggesting that these two SIM mutations have little or no effect on Mre11-6HA protein stability during vegetative growth.

Our results also indicate that, in the absence of MMS, the DNA damage checkpoint was activated at T55 and T235 in *mre11*^{I9R}*-6HA* but not in *MRE11-6HA* or *mre11*^{I158R}*-6HA*, as a proportion of the Rad53 proteins had become hyperphosphorylated and migrated more slowly in an SDS-PAGE gel (Figure 2D, middle panel). In the presence of 0.01% MMS, the hierarchy for the DNA damage checkpoint responses was *mre11*^{I9R}*-6HA* > *mre11*^{I158R}*-6HA* > *MRE11-6HA*. In contrast, in the presence of 0.033% MMS, the DNA damage checkpoint responses in all three strains were distinctly activated at T55. The activated checkpoint in *MRE11-6HA* was then attenuated at T235, as the majority of the Rad53 proteins became unphosphorylated. Hyperphosphorylated Rad53 was still detected in *mre11*^{I158R}*-6HA* at T235 (Figure 2D, middle panel). These results suggest that *mre11*^{I9R}*-6HA* cannot repair both spontaneous and MMS-induced DSBs due to its defect in MRX assembly. The *mre11*^{I158R}*-6HA* mutant, compared to *MRE11-6HA*, is partly defective in repairing MMS-induced DSBs.

The results of PFGE (Figure 2C) are also consistent with those of MMS sensitivity (Figure 1B) and checkpoint activation (Figure 2D); the tendency for recovery of MMS-induced replication fork stalls is *MRE11-6HA* > *mre11*^{I158R}*-6HA* > *mre11*^{I9R}*-6HA*. Due to the presence of forks and bubbles that impede chromosome migration, the incompletely replicated chromosomes did not enter the gel at T55 (Figure 2C, lanes 8, 14, 17 and 26). Chromosome replication was recovered and almost completed in *MRE11-6HA* at T235 (Figure 2C, lane 9), enabling the chromosomes to enter the gel. In contrast, a significant proportion of the chromosomes was never completely replicated in *mre11*^{I9R}*-6HA* and *mre11*^{I158R}*-6HA* at T235 (Figure 2C, lanes 18 and 27).

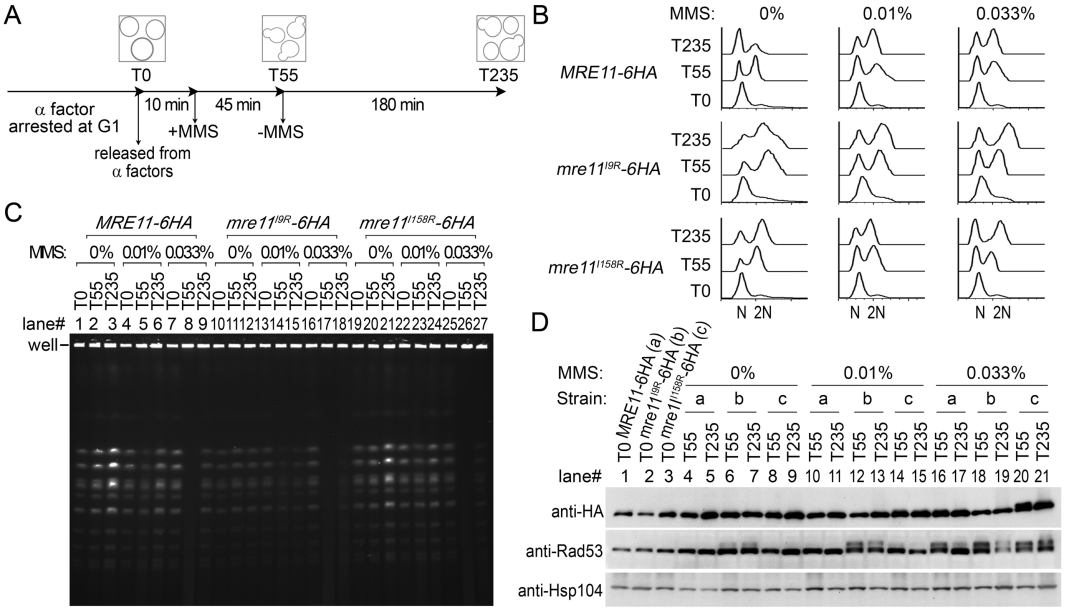

Figure 2. DNA replication during recovery from MMS-induced stalling. (**A**) Yeast cells were grown to mid-log phase, arrested in G1 by the presence of α-factor (i.e. T0) and then released from G1 arrest into YPD. After 10 min, MMS (0, 0.01% or 0.033%) was added for 45 min (i.e. T55). Cells were then washed extensively and incubated in YPD at 30°C for an additional 180 min (i.e. T235). Samples were taken at three different time points: T0 (lanes 1, 4, 7, 10, 13, 16, 19, 22 and 25), T55 (lanes 2, 5, 8, 11, 14, 17, 20, 23 and 26) and T235 (lanes 3, 6, 9, 12, 15, 18, 21, 24 and 27). (**B**) Progression of DNA replication. Yeast cells were harvested at the indicated time points after being transferred into sporulation medium. The cells were then stained with SYTOX Green, and the DNA content was measured by FACS. (**C**) PFGE. Yeast chromosomes were separated by PFGE and then visualized by staining with ethidium bromide. (**D**) DNA damage checkpoint. Total protein extracts were prepared and analyzed by immunoblot using a HA antibody and a Rad53 antibody. Hsp104 was used as a loading control. Rad53 phosphorylation—an indicator of DNA damage checkpoint activation—was assayed as the phosphorylation-dependent shift of the protein.

The MRX complex associates with the conjugated Smt3 moieties (CSMs) via SIM1 and SIM2 *in vivo*

Next, we performed co-immunoprecipitation experiments to compare the capability of Mre11-6HA, Mre11^{I9R}-6HA and Mre11^{I158R}-6HA in recruiting Smt3 and/or CSMs *in vivo*. The *MRE11-6HA*, *mre11^{I9R}-6HA* and *mre11^{I158R}-6HA* vegetative cells were treated with 0.3% MMS for 90 min. These cells also expressed V5-tagged Smt3 proteins (V5-Smt3). Total cell lysates were then prepared and used to carry out immunoprecipitation. The anti-HA affinity resin was used to pull down Mre11-6HA, Mre11^{I9R}-6HA or Mre11^{I158R}-6HA. Both total cell lysates and the bound protein complexes were subjected to immunoblotting analysis with anti-HA and anti-V5 antibody, respectively. The apparent molecular weight ($Mr_{app.}$) of V5-Smt3 determined by SDS-PAGE was ≈15 000 (Figure 3A, lanes 1-3). Our results revealed that MMS induced much more V5-tagged CSMs ($Mr_{app.} \geq 30\,000$) in *MRE11-6HA* and *mre11^{I158R}-6HA* than that in *mre11^{I9R}-6HA* (Figure 3A, lanes 4–6). Since MRX is a positive regulator for DSB-induced global SUMOylation (15) and Mre11^{I9R}-6HA cannot form a functional MRX complex, the *mre11^{I9R}-6HA* mutant is defective in DSB-induced global SUMOylation. In contrast, *mre11^{I158R}-6HA*, compared to *mre11*Δ or *mre11^{I9R}-6HA*, confers higher MMS resistance (Figure 1) but still can partly repair DSBs (Figure 2), so we inferred that RPA (24) or other novel factors in *mre11^{I158R}-6HA* might promote MMS-induced SUMOylation during DSB repair.

Next, we showed that Mre11-6HA co-immunoprecipitated much more V5-tagged CSMs (but not the V5-tagged Smt3 monomers) than Mre11^{I9R}-6HA or Mre11^{I158R}-6HA in the absence (Figure 3A upper panel, lanes 7-9) or presence (Figure 3 upper panel, lanes 10-12) of 0.3% MMS. These results are consistent with those of our two-hybrid assays (Table 1), indicating that Mre11 and/or the MRX complex preferentially interact with CSMs but not the Smt3 monomer via SIM1 and SIM2.

The immunoblotting results with anti-HA antibodies (Figure 3 lower and right panel, lanes 7-12) also revealed that Mre11-6HA and Mre11^{I158R}-6HA, but not Mre11^{I9R}-6HA, are phosphorylated in response to MMS (Figure 3 lowest panels, lane 4-6, 10-12). Notably, all these three Mre11-6HA proteins exhibited similar higher mobility patterns in SDS-PAGE (Figure 3 lowest right panels, lanes 7-12), indicating that neither SIM1 nor SIM2 significantly affects Mre11 SUMOylation (11). From these results, we can infer SUMOylation of Mre11 occurs prior to the assembly of the MRX complex. Consistent with the results of our two-hybrid assays (Table 1), the results here also indicate that Mre11-dependent global SUMOylation is mediated via the Mre11-CSM ensembles rather than the SUMOylated Mre11.

Finally, the SUMOylation of two TAP (tandem affinity purification)-tagged DNA repair proteins (Rad59 and Rfa1) was profoundly affected by *mre11*Δ or *sae2*Δ (15). Using the same approach, we found that the hierarchy for the levels of SUMOylated Rad59-TAP (Figure 3B) or Rfa1-TAP (Figure 3C) in response to 0.3% MMS were *MRE11-*

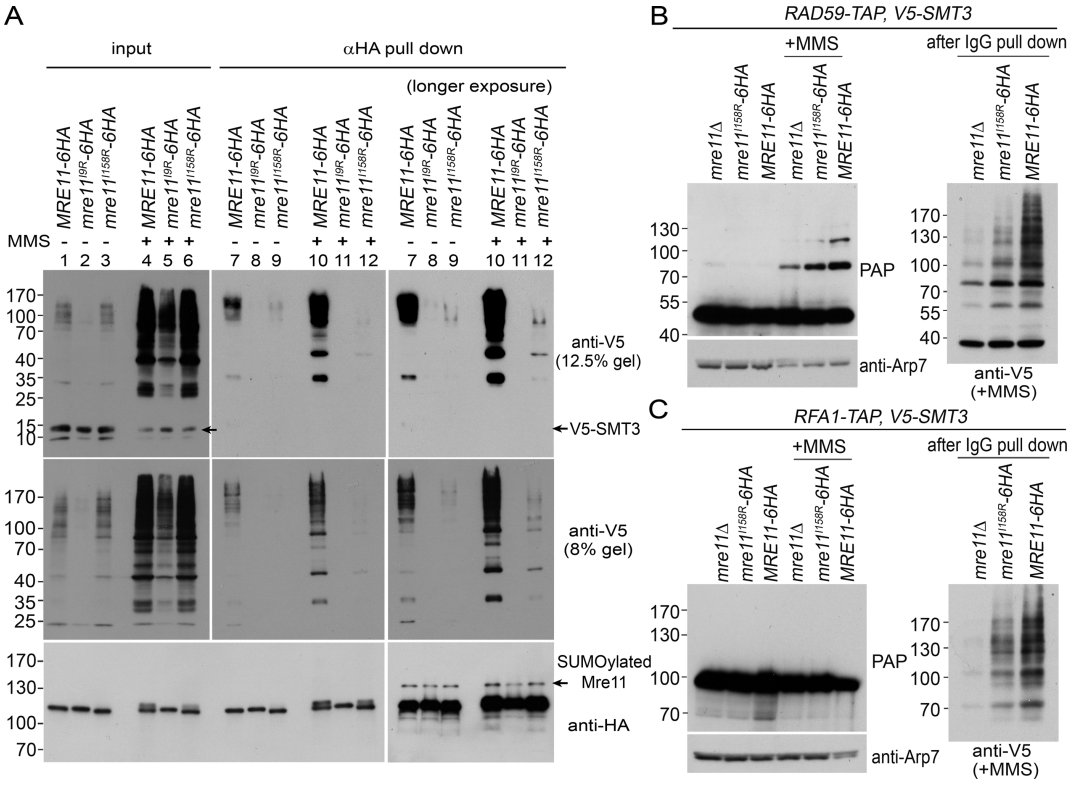

Figure 3. Mre11 promotes MMS-induced protein SUMOylation. **(A)** Mre11^{I9R}-6HA and Mre11^{I158R}-6HA mutants are defective in recruiting conjugated SUMO moieties (CSMs). Total cell lysates from vegetative cells (*MRE11-6HA V5-SMT3, mre11^{I158R}-6HA V5-SMT3 and mre11^{I9R}-6HA V5-SMT3*) untreated or treated with 0.3% MMS were prepared and used to carry out chromatin precipitation. An immobilized anti-HA affinity resin (Sigma) was used to pull down HA-tagged Mre11 proteins. The bound protein complexes and total cell lysates were subjected to immunoblotting analysis with anti-V5 antibody (top and middle panels) and anti-HA antibody (bottom panel), respectively. **(B,C)** The Mre11^{I158R}-6HA mutant is defective in promoting SUMOylation of DNA repair proteins. TAP (Tandem affinity purification)-tagged Rad59 (B) and TAP-tagged Rfa1 (C) in yeast cells untreated or treated with 0.3% MMS were analyzed by immunoblotting using the peroxidase-anti-peroxidase (PAP) antibody (left panel). TAP-tagged proteins were immunoprecipitated using IgG-Sepharose (Sigma), washed and eluted with loading buffer, before separating by SDS-PAGE and immunoblotting with anti-V5 antibodies (right panel). Arp7 was used as a loading control.

6HA > *mre11^{I158R}-6HA* > *mre11*Δ, though *mre11^{I158R}* could induce global protein SUMOylation in response to MMS (Figure 3A).

In conclusion, the wild-type vegetative cells can repair both spontaneous and MMS-induced DSBs, initiate DSB-induced global SUMOylation and maintain normal telomere length during vegetative growth. The *mre11^{I9R}* mutant fails to assemble the MRX complex, and thus it is defective in all physiological functions of the MRX complex. In contrast, *mre11^{I158R}* can repair spontaneous DSBs and maintain normal telomere length, while it is partly defective in repairing MMS-induced DSBs and thus confers higher MMS resistance than *mre11^{I9R}* and *mre11*Δ. Finally, the *mre11^{I158R}* mutant can induce global SUMOylation in response to MMS, but is less efficient than the wild-type cells in promoting SUMOylation of DNA repair proteins.

Mre11^{I9R} and Mre11^{I158R} differentially affect the formation of Spo11-induced DSBs

S. cerevisiae MRX is required for both initiation and processing of Spo11-induced DSBs (25,26). To reveal the meiotic functions of Mre11^{SIM1} and Mre11^{SIM2}, we constructed three SK1 diploid strains: *MRE11-6HA*, *mre11^{I9R}-6HA* and *mre11^{I158R}-6HA*. Tetrad dissection analyses revealed that *MRE11-6HA* generated many viable spores (>97%), whereas *mre11^{I9R}-6HA* and *mre11^{I158R}-6HA* yielded no viable spores (<1%) (Table 2).

All yeast strains were then induced to undergo relatively synchronous meiosis in the sporulation medium (SPM). At the indicated time points, cells were harvested to monitor key meiotic events as described previously (11,37). First, the FACS results indicate that these three strains exhibited no apparent differences in their completion of premeiotic DNA replication, as the majority of cells (>80%) became 4N at the 6h time point (Figure 4A). Second, we performed 4, 6-diamidino-2-phenylindole (DAPI) staining to monitor if meiotic progress in terms of MI nuclear division was delayed in *mre11^{I9R}-6HA* and *mre11^{I158R}-6HA*. The completion of MI nuclear division took about ≈4.5 h for 50% *MRE11-6HA* and ≈6.0 h for 50% *mre11^{I9R}-6HA* or 50% *mre11^{I158R}-6HA* cells, respectively. Moreover, more *mre11^{I9R}-6HA* (45%) and *mre11^{I158R}-6HA* (40%) than *MRE11-6HA* (≈15%) never underwent MI nuclear division (Figure 4B).

Next, we examined DSB formation at *YCR047C*, a DSB hot spot on chromosome III. To more precisely quantify to the level of Spo11-induced DSBs, we introduced

Table 2. Sporulation efficiency and spore viability

Strain	Sporulation				Spore viability
	Ascus with 4, 3, 2, 1 and 0 spores				
	4	3	2	1 or 0	
MRE11–6HA	69%	4%	20%	8%	98% ($n = 208$)
mre11^{I9R}-6HA	4%	6%	39%	53%	0% ($n = 112$)
mre11^{I158R}-6HA	2%	2%	50%	48%	0% ($n = 52$)
mre11^{P84S}-6HA	49%	5%	21%	25%	89% ($n = 212$)
mre11^{T188I}-6HA	4%	4%	33%	59%	0% ($n = 128$)
mre11$^{P84S, T188I}$(mre11S)-6HA	1%	3%	13%	83%	0% ($n = 52$)
*MRE11–6HA, sae2*Δ	4%	3%	33%	60%	1% ($n = 104$)
*mre11^{I9R}-6HA, sae2*Δ	0%	2%	29%	69%	n.d.*
*mre11^{I158R}-6HA, sae2*Δ	1%	3%	30%	68%	0% ($n = 58$)
SAE2–3HA	68%	5%	17%	10%	99%($n = 216$)
sae2^{K97R}-3HA	66%	3%	22%	9%	99% ($n = 208$)
sae2^{K319R}-3HA	67%	2%	18%	13%	96% ($n = 216$)
sae2$^{K97R, K319R}$-3HA	64%	3%	19%	14%	99% ($n = 216$)

Sporulation efficiencies were counted after 5 days on sporulation media at 30°C. To score for spore viability, only tetrads (but not dyads or triads) were dissected on YPD. *n.d. (not determined).

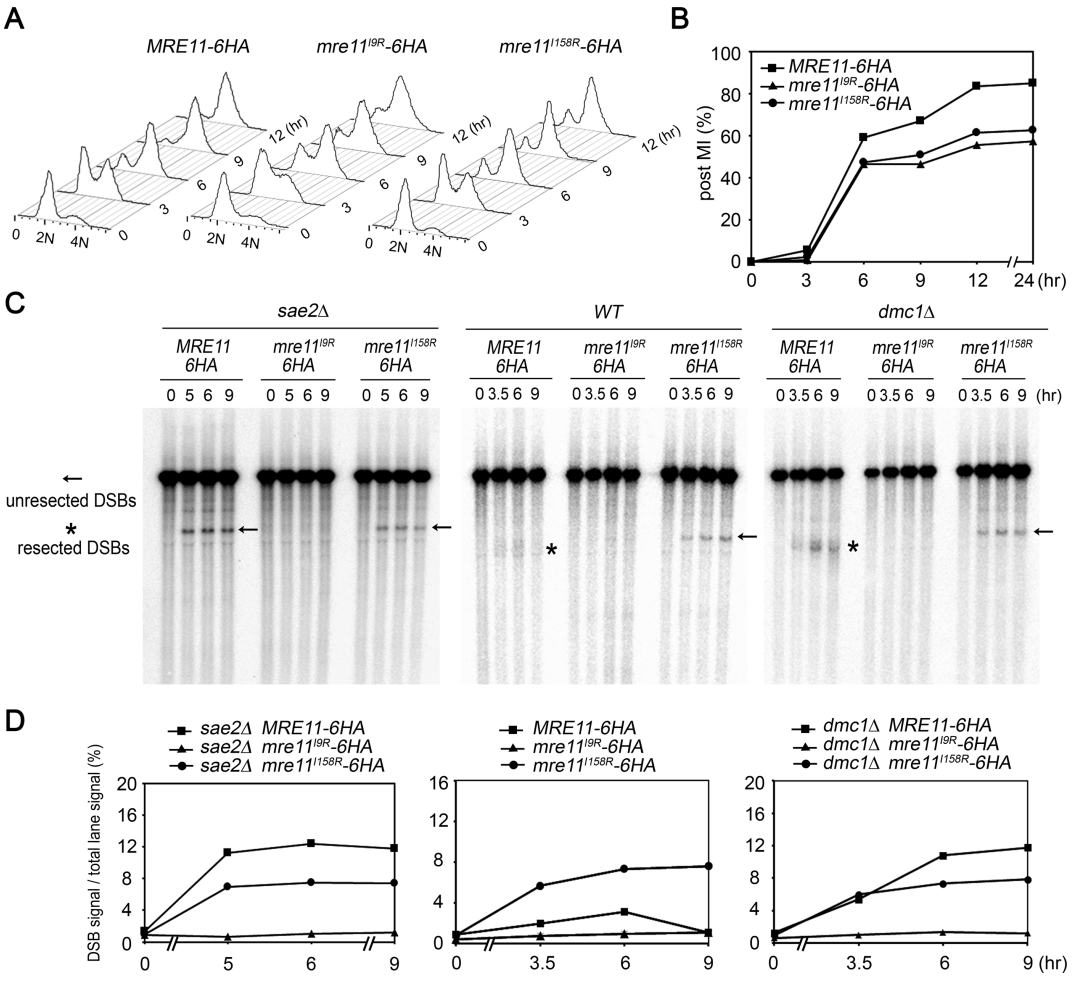

Figure 4. Pre-meiotic DNA replication, initiation and resection of Spo11-induced DSBs. (**A**) Progression of pre-meiotic DNA replication. Yeast cells were harvested at the indicated time points after being transferred into sporulation medium. The cells were then stained with SYTOX Green, and the DNA content was measured by FACS. (**B**) Timing of nuclear division (MI). The number of DAPI–stained foci per cell ($n = 200$) was counted for each time point after transfer of cells into sporulation medium (SPM). (**C, D**) Detection of DNA double strand breaks (DSBs) at the *YCR047C* –a DSB hot spot on chromosome III. Yeast genomic DNAs were digested by *Bgl*II, separated by electrophoresis on a 1% agarose gel, probed with *YOR052W* and visualized using a Fujifilm phosphorimager. Unresected DSBs at *YOR047C* DSB are indicated by arrows and those resected are indicated by an asterisk on the right, respectively. DSB signal/total lane signal ratio from the Southern blot as in (C) are shown (D).

the *sae2*Δ (*com1*Δ) mutation into these three strains. The *sae2*Δ mutant (20,70,71), like *rad50S* (72) and *mre11S* (73), blocks the resection of Spo11-induced DSBs into 3′-end ssDNA tails. Genomic DNA isolated from sporulating cultures at various time points was digested with *Bgl*II, separated by gel electrophoresis, blotted and hybridized with the *YCR052W* DNA probe as described before (11) (Figure 4C). The order for the maximum overall quantity of DSBs at this specific site was *MRE11-6HA* (≈3%), *mre11^{I9R}-6HA* (<1%), *mre11^{I158R}-6HA* (≈7%), *MRE11-6HA sae2*Δ (≈12%), *mre11^{I9R}-6HA sae2*Δ (<1%) and *mre11^{I158R}-6HA sae2*Δ (≈7%) (Figure 4D).

The overall levels of Spo11-induced DSBs along chromosome IV were also revealed by PFGE (Figure 5A) and Southern hybridization using a *FDC1* DNA probe (Figure 5B). The results further confirm that *mre11^{I9R}-6HA* is defective in the formation of Spo11-induced DSBs because *mre11^{I9R}-6HA sae2*Δ, compared to *MRE11–6HA sae2*Δ or *mre11^{I158R}-6HA sae2*Δ, accumulated much less unresected *FDC1*-containing chromosome fragments (Figure 5B, left panel). This conclusion is also supported by the results of immunoblot time course analyses using antibodies specifically against phosphorylated Hop1-T318 and phosphorylated Zip1-S75 (Figure 6). We found that *mre11^{I9R}-6HA* (Figure 6A, middle panels) and *mre11^{I9R}-6HA sae2*Δ (Figure 6B, middle panels) generated very low levels of phosphorylated Hop1-T318 and phosphorylated Zip1-S75. In contrast, more phosphorylated Hop1-T318 and Zip1-S75 proteins appeared in *MRE11-6HA*, *mre11^{I158R}-6HA* (Figure 6A), *MRE11-6HA sae2*Δ and *mre11^{I158R}-6HA sae2*Δ at the 3 h time point and thereafter (Figure 6B).

Mre11^{I158R} is phenotypically similar to *sae2*Δ, but not *dmc1*Δ, in processing of Spo11-induced DSBs

Next, we introduced the *dmc1*Δ mutation into these three strains to show that *mre11^{I158R}* is phenotypically equal to *sae2*Δ during meiosis. Unlike *sae2*Δ, the *dmc1*Δ mutant removes the Spo11-oligonucleotide complex from meiotic DNA and accumulates unrepaired 3′-end ssDNA tails (74). We found that *MRE11-6HA dmc1*Δ cells accumulate shorter, *YCR052W*-containing *Bgl*II digested DNA fragments due to excessive DSB resection (Figure 4C, right panel). In contrast, the meiotic DSBs at *YCR047C* were not resected in *mre11^{I158R}-6HA dmc1*Δ (right panel) *as in mre11^{I158R}-6HA* (middle panel) or in *mre11^{I158R}-6HA sae2*Δ (left panel). The order for the overall quantity of DSBs at *YCR047C* was *MRE11-6HA dmc1*Δ (≈12%), *mre11^{I9R}-6HA dmc1*Δ (<1%) and *mre11^{I158R}-6HA dmc1*Δ (≈7%) (Figure 4D, right panel).

The results of PFGE (Figure 5A, right panel) and Southern hybridization (Figure 5B, right panel) also indicate that *MRE11-6HA dmc1*Δ cells accumulate high levels of shorter, *FDC1*-containing chromosome fragments due to both multiple breaks and excessive DSB resection. In contrast, *mre11^{I158R}-6HA dmc1*Δ (right panel), as for *MRE11-6HA sae2*Δ (left panel) and *mre11^{I158R}-6HA sae2*Δ (right and left panels), accumulated longer and unresected *FDC1*-containing chromosome fragments (Figure 5B). We conclude that *mre11^{I158R}-6HA*, like *sae2*Δ, blocks the resection of Spo11-induced DSB ends.

Our conclusion is further supported by the results of immunoblot time course analyses (Figure 6) because only Tel1^{ATM} (but not Mec1^{ATR}) was activated in *mre11^{I158R}-6HA* as in *sae2*Δ and *rad50S* (12,36,53). Tel1^{ATM} is recruited by the MRX complex to unresected DSBs, whereas Mec1^{ATR} is recruited to replication protein A (RPA)-coated ssDNA tails. The hierarchy for the steady-state levels of phosphorylated Hop1-T318 and phosphorylated Zip1-S75 was *MRE11-6HA SAE2* > *MRE11-6HA sae2*Δ ≅ *mre11^{I158R}-6HA* ≅ *mre11^{I158R}-6HA sae2*Δ (Figure 6A-C) and *MRE11-6HA dmc1*Δ >> *mre11^{I158R}-6HA dmc1*Δ ≅ *mre11^{I158R}-6HA sae2*Δ ≅ *mre11^{I158R}-6HA* (Figure 6E). Due to the lack of 3′-end ssDNA tails in *mre11^{I158R}-6HA* (Figure 6A,E), *mre11^{I158R}-6HA sae2*Δ (Figure 6B,E) and *mre11^{I158R}-6HA dmc1*Δ (Figure 6E), these three strains accumulated low but detectable levels of phosphorylated Hop1-T318 and Zip1-S75 proteins. In contrast, both Hop1-T318 and Zip1-S75 were hyperphosphorylated in the sporulating *MRE11-6HA dmc1*Δ cells (Figure 6E, right panels). Therefore, *mre11^{I158R}*, as for *sae2*Δ or *rad50S*, does not affect Xrs2-dependent Tel1^{ATM} activation, further confirming that the MRX complex is properly assembled in *mre11^{I158R}*. Notably, all four strains (Figure 6E) produced similar levels of phosphorylated H2A-S129 (γH2A) during meiosis. H2A-S129 phosphorylation occurs during the onset of pre-meiotic DNA replication and is independent of Spo11-induced DSBs (12). In contrast, the levels of γH2A were much reduced in *mre11^{I9R}-6HA sae2*Δ (Figure 6B,C) due to the lack of properly assembled MRX complex.

Mre11 and Mre11^{I158R}, but not Mre11^{I9R}, are phosphorylated during meiosis

Notably, before they were transferred to the sporulation medium (i.e. 0-h), all Mre11-6HA proteins in the three strains exhibited the same mobility in an SDS-PAGE gel (Figure 3A,B, upper panel). Mre11^{I9R}-6HA exhibited the same mobility throughout sporulation, whereas Mre11-6HA and Mre11^{I158R}-6HA were post-translationally modified at the 3-h time point and thereafter, migrated more slowly in the SDS-PAGE gel. A dephosphorylation assay was performed as described previously (54) using calf intestinal alkaline phosphatase (CIAP) and 2-glycerophosphate (2-GP), a general phosphatase inhibitor. The results reveal that the faster and slower migrating species represent nonphosphorylated and phosphorylated proteins, respectively (Figure 6D). These results suggest that Mre11 phosphorylation occurs in the context of the MRX complex but is independent of Mre11^{SIM2}. Although Mre11 is a SUMOylated protein during vegetative growth (Figure 3A, lowest right panel), we hardly detected any SUMOylated Mre11-6HA or Mre11^{I158R}-6HA in meiotic cells by immunoblotting (Figure 6A,B).

The steady-state levels of these three HA-tagged Mre11 proteins in meiosis were also compared by cycloheximide shut-off experiments (Supplementary Figure S1B). Protein synthesis was inhibited by 200 μg/ml of cycloheximide added into the meiotic cultures at the 3-h time point. Samples were taken at 30, 60, 90, 120 and 180 min after the addition of cycloheximide (Supplementary Figure S1B, lower panel). We found that Mre11^{I9R}-6HA ($t_{1/2}$ ≈40

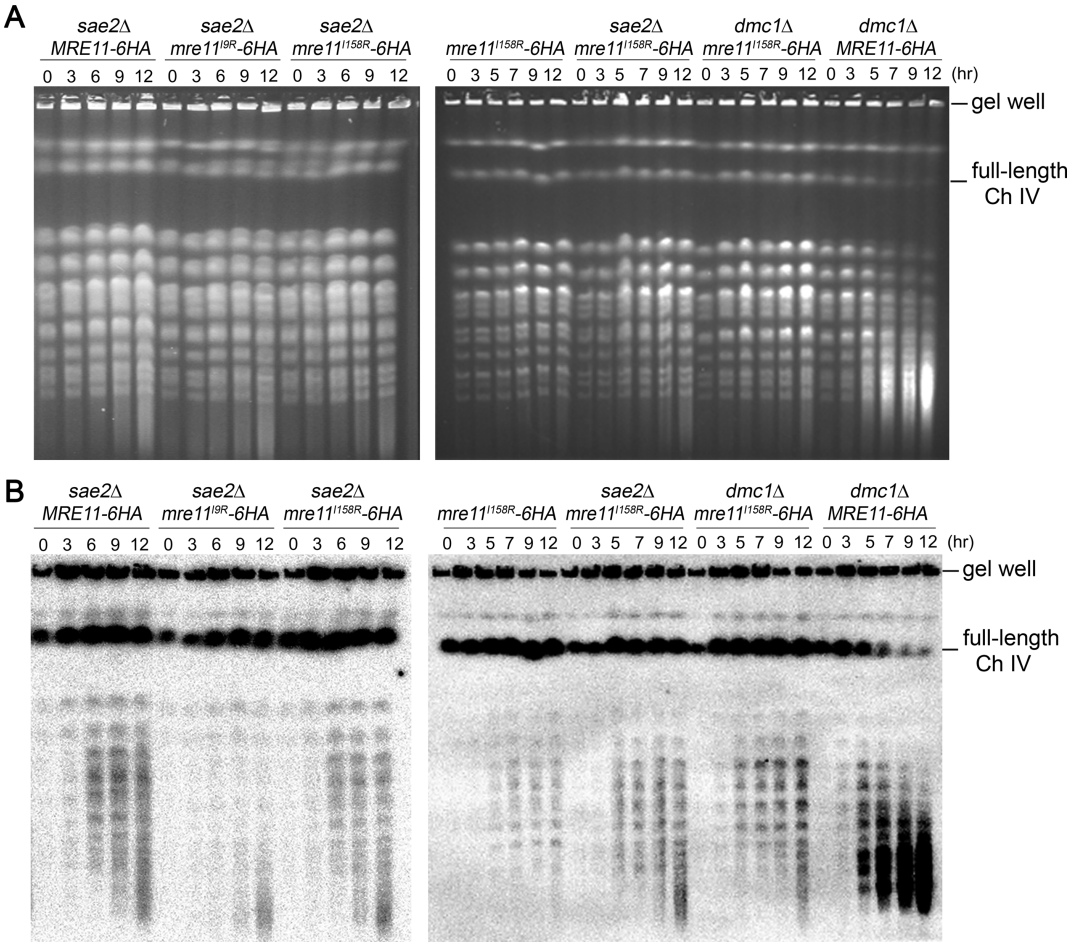

Figure 5. The overall distribution of Spo11-induced DSBs along chromosome IV. Yeast chromosomes were separated by PFGE (**A**), analyzed by Southern hybridization with a *FDC1* (*YDR539W*) DNA probe and visualized using a Fujifilm phosphorimager (**B**). All sporulation time-course experiments were repeated twice, and the representative results are shown.

min) is less stable than Mre11-6HA ($t_{1/2}$ ≈60 min) and Mre11^{I158R}-6HA ($t_{1/2}$ ≈70 min). These results might account for the lower steady-state levels of Mre11^{I9R}-6HA protein in *mre11^{I9R}-6HA* (Figure 6A, upper panel) and *mre11^{I9R}-6HA sae2*Δ (Figure 6B, upper panel) after 6-h in SPM.

A comparison between *mre11^{I158R}* and *mre11S*

Our results indicate that *mre11^{I158R}* allows initiation but not processing and repair of Spo11-induced DSBs similar to *sae2*Δ, *rad50S* and *mre11S*. The *mre11S* allele contains two point mutations, P84S and T188I (73). P84 and T188 are evolutionarily conserved. In the *S. pombe* Mre11-Nbs1 complex crystal structure (58), P93 and S207 (the amino acid equivalents of P84 and T188) reside nearby SIM1 and SIM2, respectively (Supplementary Figure S2). However, neither Mre11^{P84S} nor Mre11^{T188I} exhibit apparent defects in two-hybrid interactions with Smt3, Ubc9, Siz2, Xrs2 or Rad50 (Table 1). We found that the *S. cerevisiae mre11^{P84S}-6HA* homozygous diploid, like the *S. pombe mre11^{P93S}* homozygous diploid (75), displayed no apparent (or modest) defects in sporulation or spore viability (≈89%). In contrast, *mre11^{T188I}-6HA* and *mre11S-6HA* (*mre11$^{P84S, T188I}$-6HA*) are unable to produce any viable spore (Table 2). Therefore, the T188I mutation is the main cause for *mre11S* (64). As *S. cerevisiae* T188 and *S. pombe* S207 are located in a surface loop that contains conserved positively-charged residues critical for DNA binding (Supplementary Figure S2), the T188I mutation might distort Mre11 DNA binding during processing of meiotic DSBs (58,64,76). Since T188, as for *S. pombe* S207 (58), is close to SIM2, we speculated that the Mre11^{SIM2}-CSM interaction might affect the Mre11 DNA binding during meiosis. Next, we carried out meiotic nuclear spread immunostaining experiments to determine whether Mre11-6HA, Mre11^{I9R}-6HA and Mre11^{I158R}-6HA were properly targeted to meiotic chromosomes using the anti-HA antisera (Figure 7A). It is known that *sae2*Δ or *rad50S* accumulate Mre11 foci, which is not seen in the wild type (27). Our cytology data (Figure 7B) revealed that the Mre11-6HA foci appeared at the 3.5-h sporulation time point in wild-type and *sae2*Δ, but only persisted at the 5-h sporulation time point in *sae2*Δ. Neither of these two strains examined here formed Mre11^{I9R}-6HA foci because Mre11^{I9R}-6HA is unable to assemble the MRX complex. In contrast, Mre11^{I158R}-6HA foci accumulated in both wild-type and *sae2*Δ, indicating that the Mre11^{SIM2}-

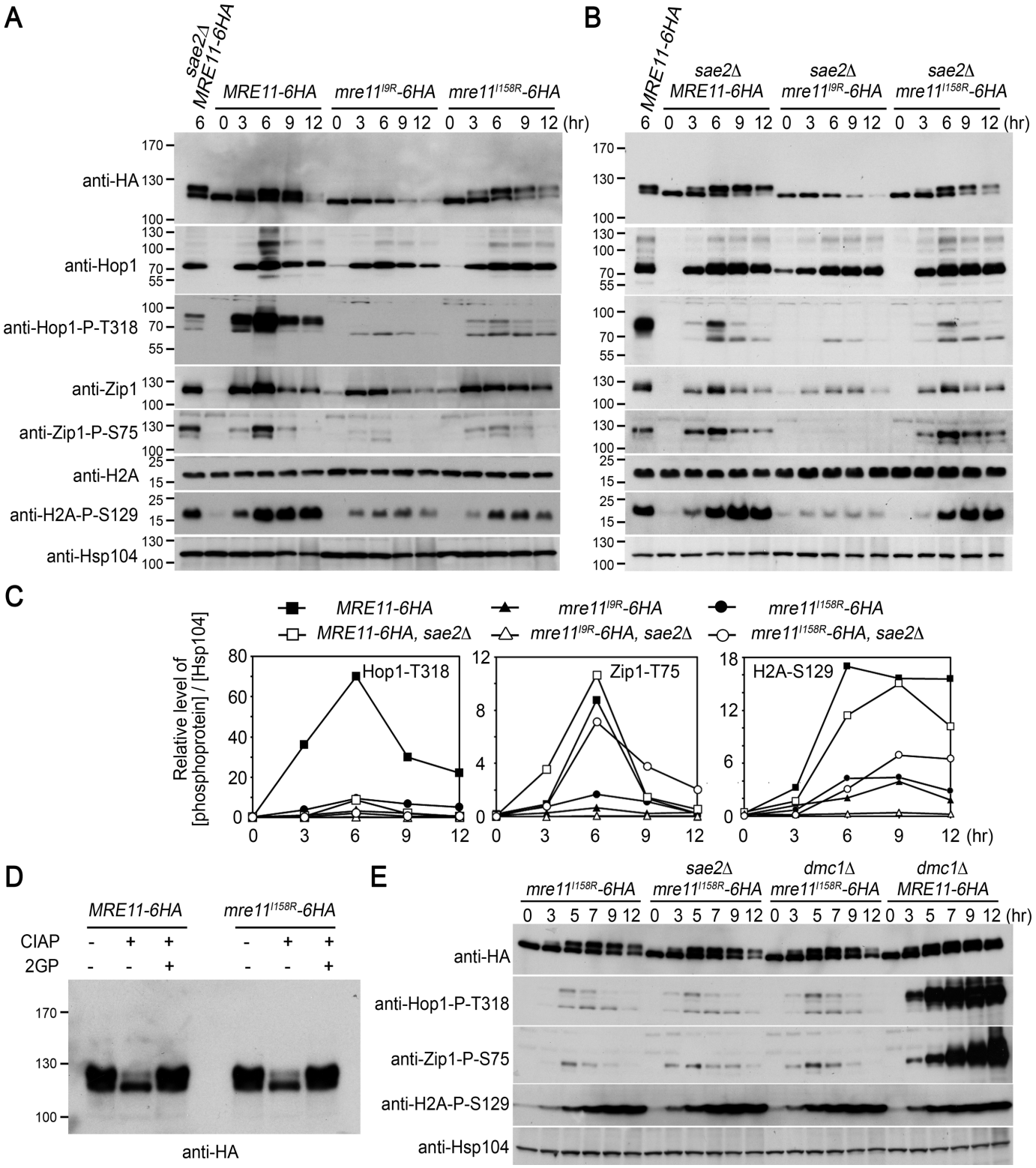

Figure 6. Meiotic checkpoint activation. (**A, B**) Immunoblotting time-course analysis of yeast cells in wild-type (A) and *sae2*Δ (B) backgrounds. All of the antibodies used have been described previously (12,36,54). Hsp104 was used as a loading control. (**C**) Quantitation of immunoblotting results in (A and B) was determined as previously described. The relative levels of different phosphoprotein versus Hsp104 (loading control) at each time point are shown. (**D**) Gel mobility shift analysis. Total cell lysates of meiotic cells at 6 h after being transferred into sporulation medium were treated with calf intestinal alkaline phosphatase (CIAP; 120U) in the absence or presence of 2-glycerophosphate (2PG; 16 mM). (**E**) Western blot time-course analysis of *MRE11-6HA* and *mre11*^{I158R}*-6HA* in *sae2*Δ and *dmc1*Δ backgrounds.

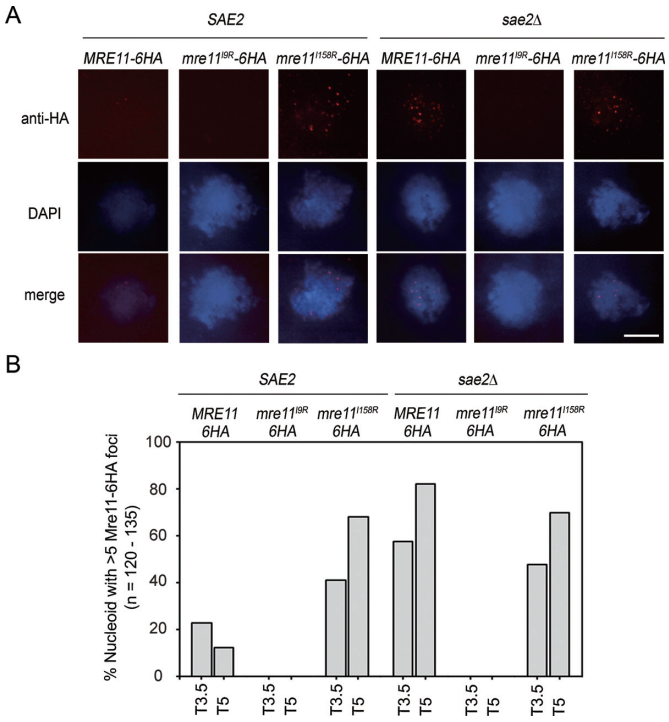

Figure 7. Accumulation of Mre11^{I158R}-6HA foci along meiotic chromosomes in the wild-type and *sae2*Δ meiotic cells. (**A**) Nucleoids prepared at indicated meiotic time points were stained by anti-HA serum (red1) and DAPI (blue). Representative images are shown. The white bar represents 5 μm. (**B**) Quantitation of Mre11–6HA, Mre11^{I9R}-6HA and Mre11^{I158R}-6HA foci per nucleoids meiotic time points (A and B). The percentage of nucleoids with more than five anti-HA positive foci was obtained from 120–150 randomly selected nucleoids.

CSM interaction is dispensable for the Mre11 DNA binding during meiosis. It is of interest to further determine how the Mre11^{SIM2}-CSM interaction affects the catalytic function of Mre11 in processing Spo11-induced DSBs.

Mre11 is unlikely to recruit SUMOylated Sae2 for end processing of Spo11-induced DSBs

Sae2 can directly interact with Mre11 (77) and the MRX complex (30) *in vitro*. There are two putative SUMOylation sites (K97 and K319) in Sae2. The SUMOylation at K97 of Sae2 increases both soluble Sae2 and the MRX function in dsDNA end resection during vegetative growth (21). We postulated that Mre11^{SIM2} might recruit SUMOylated Sae2 to reconstitute a functional MRX-Sae2 dsDNA endonuclease (at least) during vegetative growth. However, this hypothesis is not applicable to the repair of Spo11-induced DSBs: (i) Sae2 SUMOylation might not occur *in vivo* during meiosis because SUMOylated Sae2-3HA was not detected in meiotic cells by immunoblot time course experiments (Supplementary Figure S3). (ii) Both *sae2^{K97R}-3HA* (21) and *sae2$^{K97R,\ K319R}$-3HA* mutants, as compared to wild-type *SAE2-3HA* diploid cells, underwent normal sporulation and produced (>90%) viable spore (Table 2). (iii) It has been reported that the phosphorylation of Sae2 is required to initiate resection and to improve the efficiency of resection through cooperation with the MRX complex during meiosis (78,79). Our results also confirm that Sae2-3HA, Sae2^{K97R}-3HA and Sae2^{K97R,K319R}-3HA are phosphorylated during meiosis (Supplementary Figure S3).

DISCUSSION

The results in this report indicate that *S. cerevisiae* Mre11 can non-covalently recruit CSMs (particularly the poly-SUMO chains or their conjugates) to facilitate its assembly and functions during both vegetative growth and meiosis. Mre11 first recruits CSMs via SIM1 to facilitate MRX assembly and/or Mre11 folding, after which, Mre11 recruits CSMs via SIM2 to promote its interaction with the SUMO enzymes (E2/Ubc9 and E3/Siz2). These enzymes then induce global SUMOylation at DSB sites, particularly SUMOylation of DNA repair enzymes. However, the Mre11^{SIM2}-CSM interaction does not affect Xrs2-dependent Tel1 activation. We also show that the primary defect of the *mre11^{I158R}* mutation, as for *rad50S*, *sae2*Δ and *mre11S*, is to block the resection of the Spo11-induced DSB ends during meiosis. Mre11^{SIM1} and Mre11^{SIM2} are evolutionarily conserved in *S. cerevisiae* and *S. pombe*. It would be interesting to investigate further whether the *S. pombe* Mre11^{SIM1} and Mre11^{SIM2} are also important for the assembly of MRN and/or its function in mitosis and meiosis.

Our results support the hypothesis that CSMs can non-covalently prevent premature aggregation by increasing the water solubility of individual protein subunits (8,9) prior to their assembly into a functional MRX complex (10,11,37). Similar to this scenario, SUMOylation of Sae2 increases both soluble Sae2 and the Sae2's function in DNA end resection (21). To coordinate this task in a timely manner, these CSMs or SUMOylation are negatively regulated by deSUMOylation proteases and SUMO-targeted ubiquitin ligases. Consistent with this, mutations in either deSUMOylation protease genes (*ulp1^{ts}*, *ulp2*Δ) (16,17) or SUMO-targeted ubiquitin ligase genes (*slx5*Δ, *slx8*Δ) (18,19) cause pronounced effects on DSB repair and genomic instability. Accordingly, we suggest that the SIM2-dependent MRX-CSM interaction can provide a regulatory function in regulating MRX function during DSB repair.

A key finding of this study is that SUMOylation of *S. cerevisiae* Mre11 is unlikely to be required for the formation of the MRX complex and the DSB-induced SUMOylation of DNA repair proteins (Figure 3A). Mre11-6HA, Mre11^{I9R}-6HA and Mre11^{I158R}-6HA all can be SUMOylated during vegetative growth. However, we failed to detect SUMOylated Mre11–6HA by immunoblotting during meiosis (Figure 6). Our results also indicate that Mre11-6HA and Mre11^{I158R}-6HA, but not Mre11^{I9R}-6HA, are phosphorylated and can form MRX complexes during both vegetative growth and meiosis. Because Mre11^{I9R}-6HA is unable to form an MRX complex, we further inferred that Mre11 SUMOylation and phosphorylation occur before and after Mre11 assembly, respectively. Further investigation will reveal whether phosphorylation of Mre11 is functionally relevant to MRX assembly, DSB-dependent checkpoint activation or global SUMOylation.

SUMOylation of Sae2 increases both soluble Sae2 and the MRX function in DNA end resection during vegetative growth (21). Our results have revealed that SUMOylated

Sae2 protein not only was not detected by immunoblotting but also that it is functionally unimportant for meiosis, sporulation and spore viability (Supplementary Figure S3 and Table 2). Like Mre11, Sae2 is also a phosphorylated protein during meiosis. Phosphorylation of Sae2 Ser-267 by cyclin-dependent kinase 1 (Cdk1) is required to initiate meiotic DSB resection by allowing Spo11 removal from DSB ends (78,79). It is still unclear how phosphorylated Sae2 regulates the Sae2-Mre11 interaction. In *S. pombe*, Ctp1 is the functional counterpart of Sae2 in *S. cerevisiae* and CtIP in mammals (80). Sae2, Ctp1 and CtIP share limited homology (approximately 30 amino acids) at their C-terminal RHR motifs (80), which are responsible for dsDNA binding (81). Ctp1 also is referred to as an Nbs1 interacting protein (Nip1) because Nbs1 recruits phosphorylated Ctp1 to DSBs via its binding to the Nbs1 FHA domain of Ctp1 phosphorylated SXT motifs (Ctp1 residues 71-79) (82,83). In contrast, Sae2 interacts with Mre11 but not Xrs2 (77). Furthermore, the SXT motif is not conserved in Sae2. The coupling mechanism between MRX and Sae2 in *S. cerevisiae* may be different from that of MRX and Ctp1 in *S. pombe*.

Finally, we previously proposed that the meiosis-specific axial protein Red1 might recruit CSMs to activate Tel1 for Spo11-dependent Hop1 (or Hop1-T318) phosphorylation (11,12). The results in this report indicate that the Red1-CSM complex does not exert this function via an interaction with Mre11 (or the SIM2 in Mre11), because Xrs2-dependent Tel1 activation still occurs in the $mre11^{I158R}$ diploid during meiosis (Figure 6A). We intend to conduct further studies to decipher the coupling mechanism between Red1 and Tel1.

SUPPLEMENTARY DATA

Supplementary Data are available at NAR Online.

ACKNOWLEDGEMENTS

We thank Lorraine S. Symington (Columbia University College of Physician and Surgeons, New York, USA) for the $mre11^{D16A}$ and *mre11*Δ mutants, Xiaolan Zhao (Memorial Sloan-Kettering Cancer Center, New York, USA), Maria Pia Longhese (Università degli Studi di Milano-Bicocca, Milan, Italy) for the *SAE2–3HA* strains, Franz Klein (Max F. Perutz Laboratories, Vienna, Austria) for the $mre11^{P84S}$ haploid strain and John O'Brien (IMB, Academia Sinica) for editing the manuscript.

Author contributions: Y.J.C., Y.C.C., C.N.C. and Y.H.C. performed the experiments and analyzed the data. T.F.W. conceived and designed the experiments. T.F.W., Y.C.C. and Y.J.C. wrote the paper. All authors read and approved the manuscript.

FUNDING

Funding for open access charge: Academia Sinica and the Ministry of Science Technology (101-2311-B-001-018-MY3, 103-2311-B-001-031-MY3), Taiwan, Republic of China [T.F.W.]; Y.J.C. carried out his thesis research under the auspices of the Graduate Program of Biotechnology in Medicine, National Tsing Hua University and the National Health Research Institutes. Y.Y.C. was supported by a postdoctoral fellowship from Academia Sinica.

Conflict of interest statement. None declared.

REFERENCES

1. Hay,R.T. (2005) SUMO: a history of modification. *Mol. Cell*, **18**, 1–12.
2. Meulmeester,E. and Melchior,F. (2008) Cell biology: SUMO. *Nature*, **452**, 709–711.
3. Ulrich,H.D. (2008) The fast-growing business of SUMO chains. *Mol. Cell*, **32**, 301–305.
4. Song,J., Durrin,L.K., Wilkinson,T.A., Krontiris,T.G. and Chen,Y. (2004) Identification of a SUMO-binding motif that recognizes SUMO-modified proteins. *Proc. Natl. Acad. Sci. U.S.A.*, **101**, 14373–14378.
5. Danielsen,J.R., Povlsen,L.K., Villumsen,B.H., Streicher,W., Nilsson,J., Wikstrom,M., Bekker-Jensen,S. and Mailand,N. (2012) DNA damage-inducible SUMOylation of HERC2 promotes RNF8 binding via a novel SUMO-binding Zinc finger. *J. Cell Biol.*, **197**, 179–187.
6. Hay,R.T. (2013) Decoding the SUMO signal. *Biochem. Soc. Trans.*, **41**, 463–473.
7. Psakhye,I. and Jentsch,S. (2012) Protein group modification and synergy in the SUMO pathway as exemplified in DNA repair. *Cell*, **151**, 807–820.
8. Mossessova,E. and Lima,C.D. (2000) Ulp1-SUMO crystal structure and genetic analysis reveal conserved interactions and a regulatory element essential for cell growth in yeast. *Mol. Cell*, **5**, 865–876.
9. Lee,C.D., Sun,H.C., Hu,S.M., Chiu,C.F., Homhuan,A., Liang,S.M., Leng,C.H. and Wang,T.F. (2008) An improved SUMO fusion protein system for effective production of native proteins. *Protein Sci.*, **17**, 1241–1248.
10. Lee,C.D., Yan,Y.P., Liang,S.M. and Wang,T.F. (2009) Production of FMDV virus-like particles by a SUMO fusion protein approach in *Escherichia coli*. *J. Biomed. Sci.*, **16**, 69.
11. Lin,F.M., Lai,Y.J., Shen,H.J., Cheng,Y.H. and Wang,T.F. (2010) Yeast axial-element protein, Red1, binds SUMO chains to promote meiotic interhomologue recombination and chromosome synapsis. *EMBO J.*, **29**, 586–596.
12. Cheng,Y.H., Chuang,C.N., Shen,H.J., Lin,F.M. and Wang,T.F. (2013) Three distinct modes of Mec1/ATR and Tel1/ATM activation illustrate differential checkpoint targeting during budding yeast early meiosis. *Mol. Cell. Biol.*, **33**, 3365–3376.
13. Dou,H., Huang,C., Van Nguyen,T., Lu,L.S. and Yeh,E.T. (2011) SUMOylation and de-SUMOylation in response to DNA damage. *FEBS Lett.*, **585**, 2891–2896.
14. Srikumar,T., Lewicki,M.C., Costanzo,M., Tkach,J.M., van Bakel,H., Tsui,K., Johnson,E.S., Brown,G.W., Andrews,B.J., Boone,C. *et al.* (2013) Global analysis of SUMO chain function reveals multiple roles in chromatin regulation. *J. Cell Biol.*, **201**, 145–163.
15. Cremona,C.A., Sarangi,P., Yang,Y., Hang,L.E., Rahman,S. and Zhao,X. (2012) Extensive DNA damage-induced sumoylation contributes to replication and repair and acts in addition to the mec1 checkpoint. *Mol. Cell*, **45**, 422–432.
16. Li,S.J. and Hochstrasser,M. (1999) A new protease required for cell-cycle progression in yeast. *Nature*, **398**, 246–251.
17. Li,S.J. and Hochstrasser,M. (2000) The yeast *ULP2* (*SMT4*) gene encodes a novel protease specific for the ubiquitin-like Smt3 protein. *Mol. Cell. Biol.*, **20**, 2367–2377.
18. Ii,T., Mullen,J.R., Slagle,C.E. and Brill,S.J. (2007) Stimulation of *in vitro* sumoylation by Slx5-Slx8: evidence for a functional interaction with the SUMO pathway. *DNA Repair*, **6**, 1679–1691.
19. Prudden,J., Pebernard,S., Raffa,G., Slavin,D.A., Perry,J.J., Tainer,J.A., McGowan,C.H. and Boddy,M.N. (2007) SUMO-targeted ubiquitin ligases in genome stability. *EMBO J.*, **26**, 4089–4101.
20. Prinz,S., Amon,A. and Klein,F. (1997) Isolation of *COM1*, a new gene required to complete meiotic double-strand break-induced recombination in *Saccharomyces cerevisiae*. *Genetics*, **146**, 781–795.
21. Sarangi,P., Steinacher,R., Altmannova,V., Fu,Q., Paull,T.T., Krejci,L., Whitby,M.C. and Zhao,X. (2015) Sumoylation influences

DNA break repair partly by increasing the solubility of a conserved end resection protein. *PLoS Genet.*, **11**, e1004899.
22. Chen,H., Donnianni,R.A., Handa,N., Deng,S.K., Oh,J., Timashev,L.A., Kowalczykowski,S.C. and Symington,L.S. (2015) Sae2 promotes DNA damage resistance by removing the Mre11-Rad50-Xrs2 complex from DNA and attenuating Rad53 signaling. *Proc. Natl. Acad. Sci. U.S.A.*, **112**, E1880–E1887.
23. Puddu,F., Oelschlaegel,T., Guerini,I., Geisler,N.J., Niu,H., Herzog,M., Salguero,I., Ochoa-Montano,B., Vire,E., Sung,P. *et al.* (2015) Synthetic viability genomic screening defines Sae2 function in DNA repair. *EMBO J.*, **34**, 1509–1522.
24. Chung,I. and Zhao,X. (2015) DNA break-induced sumoylation is enabled by collaboration between a SUMO ligase and the ssDNA-binding complex RPA. *Genes Dev.*, **29**, 1593–1598.
25. Borde,V. (2007) The multiple roles of the Mre11 complex for meiotic recombination. *Chromosome Res.*, **15**, 551–563.
26. Keeney,S. (2001) Mechanism and control of meiotic recombination initiation. *Curr. Top. Dev. Biol.*, **52**, 1–53.
27. Usui,T., Ohta,T., Oshiumi,H., Tomizawa,J., Ogawa,H. and Ogawa,T. (1998) Complex formation and functional versatility of Mre11 of budding yeast in recombination. *Cell*, **95**, 705–716.
28. Borde,V., Lin,W., Novikov,E., Petrini,J.H., Lichten,M. and Nicolas,A. (2004) Association of Mre11p with double-strand break sites during yeast meiosis. *Mol. Cell*, **13**, 389–401.
29. Neale,M.J., Pan,J. and Keeney,S. (2005) Endonucleolytic processing of covalent protein-linked DNA double-strand breaks. *Nature*, **436**, 1053–1057.
30. Cannavo,E. and Cejka,P. (2014) Sae2 promotes dsDNA endonuclease activity within Mre11-Rad50-Xrs2 to resect DNA breaks. *Nature*, **514**, 122–125.
31. Bishop,D.K. (1994) RecA homologs Dmc1 and Rad51 interact to form multiple nuclear complexes prior to meiotic chromosome synapsis. *Cell*, **79**, 1081–1092.
32. Shinohara,A., Gasior,S., Ogawa,T., Kleckner,N. and Bishop,D.K. (1997) *Saccharomyces cerevisiae recA* homologues *RAD51* and *DMC1* have both distinct and overlapping roles in meiotic recombination. *Genes Cells*, **2**, 615–629.
33. Neale,M.J. and Keeney,S. (2006) Clarifying the mechanics of DNA strand exchange in meiotic recombination. *Nature*, **442**, 153–158.
34. Lange,J., Pan,J., Cole,F., Thelen,M.P., Jasin,M. and Keeney,S. (2011) ATM controls meiotic double-strand-break formation. *Nature*, **479**, 237–240.
35. Carballo,J.A., Panizza,S., Serrentino,M.E., Johnson,A.L., Geymonat,M., Borde,V., Klein,F. and Cha,R.S. (2013) Budding yeast ATM/ATR control meiotic double-strand break (DSB) levels by down-regulating Rec114, an essential component of the DSB-machinery. *PLoS Genet.*, **9**, e1003545.
36. Chuang,C.N., Cheng,Y.H. and Wang,T.F. (2012) Mek1 stabilizes Hop1-Thr318 phosphorylation to promote interhomolog recombination and checkpoint responses during yeast meiosis. *Nucleic Acids Res.*, **40**, 11416–11427.
37. Cheng,C.H., Lo,Y.H., Liang,S.S., Ti,S.C., Lin,F.M., Yeh,C.H., Huang,H.Y. and Wang,T.F. (2006) SUMO modifications control assembly of synaptonemal complex and polycomplex in meiosis of *Saccharomyces cerevisiae*. *Genes Dev.*, **20**, 2067–2081.
38. Klug,H., Xaver,M., Chaugule,V.K., Koidl,S., Mittler,G., Klein,F. and Pichler,A. (2013) Ubc9 SUMOylation controls SUMO chain formation and meiotic synapsis in *Saccharomyces cerevisiae*. *Mol. Cell*. **50**, 625–636
39. Zhang,L., Espagne,E., de Muyt,A., Zickler,D. and Kleckner,N.E. (2014) Interference-mediated synaptonemal complex formation with embedded crossover designation. *Proc. Natl. Acad. Sci. U.S.A.*, **111**, E5059–E5068.
40. Spirek,M., Estreicher,A., Csaszar,E., Wells,J., McFarlane,R.J., Watts,F.Z. and Loidl,J. (2010) SUMOylation is required for normal development of linear elements and wild-type meiotic recombination in *Schizosaccharomyces pombe*. *Chromosoma*, **119**, 59–72.
41. De Muyt,A., Zhang,L., Piolot,T., Kleckner,N., Espagne,E. and Zickler,D. (2014) E3 ligase Hei10: a multifaceted structure-based signaling molecule with roles within and beyond meiosis. *Genes Dev.*, **28**, 1111–1123.
42. Liu,M., Shi,S., Zhang,S., Xu,P., Lai,J., Liu,Y., Yuan,D., Wang,Y., Du,J. and Yang,C. (2014) SUMO E3 ligase AtMMS21 is required for normal meiosis and gametophyte development in *Arabidopsis*. *BMC Plant Biol.*, **14**, 153.
43. Qiao,H., Prasada Rao,H.B., Yang,Y., Fong,J.H., Cloutier,J.M., Deacon,D.C., Nagel,K.E., Swartz,R.K., Strong,E., Holloway,J.K. *et al.* (2014) Antagonistic roles of ubiquitin ligase HEI10 and SUMO ligase RNF212 regulate meiotic recombination. *Nat. Genet.*, **46**, 194–199.
44. Usui,T., Ogawa,H. and Petrini,J.H. (2001) A DNA damage response pathway controlled by Tel1 and the Mre11 complex. *Mol. Cell*, **7**, 1255–1266.
45. Nakada,D., Matsumoto,K. and Sugimoto,K. (2003) ATM-related Tel1 associates with double-strand breaks through an Xrs2-dependent mechanism. *Genes Dev.*, **17**, 1957–1962.
46. Falck,J., Coates,J. and Jackson,S.P. (2005) Conserved modes of recruitment of ATM, ATR and DNA-PKcs to sites of DNA damage. *Nature*, **434**, 605–611.
47. You,Z., Chahwan,C., Bailis,J., Hunter,T. and Russell,P. (2005) ATM activation and its recruitment to damaged DNA require binding to the C terminus of Nbs1. *Mol. Cell. Biol.*, **25**, 5363–5379.
48. Navadgi-Patil,V.M. and Burgers,P.M. (2009) A tale of two tails: activation of DNA damage checkpoint kinase Mec1/ATR by the 9–1–1 clamp and by Dpb11/TopBP1. *DNA Repair (Amst.)*, **8**, 996–1003.
49. Refolio,E., Cavero,S., Marcon,E., Freire,R. and San-Segundo,P.A. (2011) The Ddc2/ATRIP checkpoint protein monitors meiotic recombination intermediates. *J. Cell Sci.*, **124**, 2488–2500.
50. Grushcow,J.M., Holzen,T.M., Park,K.J., Weinert,T., Lichten,M. and Bishop,D.K. (1999) *Saccharomyces cerevisiae* checkpoint genes *MEC1*, *RAD17* and *RAD24* are required for normal meiotic recombination partner choice. *Genetics*, **153**, 607–620.
51. Thompson,D.A. and Stahl,F.W. (1999) Genetic control of recombination partner preference in yeast meiosis. Isolation and characterization of mutants elevated for meiotic unequal sister-chromatid recombination. *Genetics*, **153**, 621–641.
52. Hong,E.J. and Roeder,G.S. (2002) A role for Ddc1 in signaling meiotic double-strand breaks at the pachytene checkpoint. *Genes Dev.*, **16**, 363–376.
53. Carballo,J.A., Johnson,A.L., Sedgwick,S.G. and Cha,R.S. (2008) Phosphorylation of the axial element protein Hop1 by Mec1/Tel1 ensures meiotic interhomolog recombination. *Cell*, **132**, 758–770.
54. Lai,Y.J., Lin,F.M., Chuang,M.J., Shen,H.J. and Wang,T.F. (2011) Genetic requirements and meiotic function of phosphorylation of the yeast axial element protein Red1. *Mol. Cell. Biol.*, **31**, 912–923.
55. Eichinger,C.S. and Jentsch,S. (2010) Synaptonemal complex formation and meiotic checkpoint signaling are linked to the lateral element protein Red1. *Proc. Natl. Acad. Sci. U.S.A.*, **107**, 11370–11375.
56. Krogh,B.O., Llorente,B., Lam,A. and Symington,L.S. (2005) Mutations in Mre11 phosphoesterase motif I that impair *Saccharomyces cerevisiae* Mre11-Rad50-Xrs2 complex stability in addition to nuclease activity. *Genetics*, **171**, 1561–1570.
57. Minty,A., Dumont,X., Kaghad,M. and Caput,D. (2000) Covalent modification of p73alpha by SUMO-1. Two-hybrid screening with p73 identifies novel SUMO-1-interacting proteins and a SUMO-1 interaction motif. *J. Biol. Chem.*, **275**, 36316–36323.
58. Schiller,C.B., Lammens,K., Guerini,I., Coordes,B., Feldmann,H., Schlauderer,F., Mockel,C., Schele,A., Strasser,K., Jackson,S.P. *et al.* (2012) Structure of Mre11-Nbs1 complex yields insights into ataxia-telangiectasia-like disease mutations and DNA damage signaling. *Nat. Struct. Mol. Biol.*, **19**, 693–700.
59. Arora,C., Kee,K., Maleki,S. and Keeney,S. (2004) Antiviral protein Ski8 is a direct partner of Spo11 in meiotic DNA break formation, independent of its cytoplasmic role in RNA metabolism. *Mol. Cell*, **13**, 549–559.
60. Bylebyl,G.R., Belichenko,I. and Johnson,E.S. (2003) The SUMO isopeptidase Ulp2 prevents accumulation of SUMO chains in yeast. *J. Biol. Chem.*, **278**, 44113–44120.
61. Gill,G. (2004) SUMO and ubiquitin in the nucleus: different functions, similar mechanisms? *Genes Dev.*, **18**, 2046–2059.
62. Bressan,D.A., Olivares,H.A., Nelms,B.E. and Petrini,J.H. (1998) Alteration of N-terminal phosphoesterase signature motifs inactivates *Saccharomyces cerevisiae* Mre11. *Genetics*, **150**, 591–600.

63. Bonetti,D., Martina,M., Clerici,M., Lucchini,G. and Longhese,M.P. (2009) Multiple pathways regulate 3′ overhang generation at *S. cerevisiae* telomeres. *Mol. Cell*, **35**, 70–81.
64. Hopfner,K.P., Karcher,A., Craig,L., Woo,T.T., Carney,J.P. and Tainer,J.A. (2001) Structural biochemistry and interaction architecture of the DNA double-strand break repair Mre11 nuclease and Rad50-ATPase. *Cell*, **105**, 473–485.
65. Mimitou,E.P. and Symington,L.S. (2009) DNA end resection: many nucleases make light work. *DNA Repair (Amst.)*, **8**, 983–995.
66. Lamarche,B.J., Orazio,N.I. and Weitzman,M.D. (2010) The MRN complex in double-strand break repair and telomere maintenance. *FEBS Lett.*, **584**, 3682–3695.
67. Williams,G.J., Lees-Miller,S.P. and Tainer,J.A. (2010) Mre11-Rad50-Nbs1 conformations and the control of sensing, signaling, and effector responses at DNA double-strand breaks. *DNA Repair*, **9**, 1299–1306.
68. Sanchez,Y., Desany,B.A., Jones,W.J., Liu,Q., Wang,B. and Elledge,S.J. (1996) Regulation of *RAD53* by the ATM-like kinases *MEC1* and *TEL1* in yeast cell cycle checkpoint pathways. *Science*, **271**, 357–360.
69. Pellicioli,A., Lucca,C., Liberi,G., Marini,F., Lopes,M., Plevani,P., Romano,A., Fiore,P.P. and Foiani,M. (1999) Activation of Rad53 kinase in response to DNA damage and its effect in modulating phosphorylation of the lagging strand DNA polymerase. *EMBO J.*, **18**, 6561–6572.
70. Keeney,S. and Kleckner,N. (1995) Covalent protein-DNA complexes at the 5′ strand termini of meiosis-specific double-strand breaks in yeast. *Proc. Natl. Acad. Sci. U.S.A.*, **92**, 11274–11278.
71. McKee,A.H. and Kleckner,N. (1997) A general method for identifying recessive diploid-specific mutations in *Saccharomyces cerevisiae*, its application to the isolation of mutants blocked at intermediate stages of meiotic prophase and characterization of a new gene *SAE2*. *Genetics*, **146**, 797–816.
72. Cao,L., Alani,E. and Kleckner,N. (1990) A pathway for generation and processing of double-strand breaks during meiotic recombination in *S. cerevisiae*. *Cell*, **61**, 1089–1101.
73. Nairz,K. and Klein,F. (1997) *mre11S*–a yeast mutation that blocks double-strand-break processing and permits nonhomologous synapsis in meiosis. *Genes Dev.*, **11**, 2272–2290.
74. Bishop,D.K., Park,D., Xu,L. and Kleckner,N. (1992) *DMC1*: a meiosis-specific yeast homolog of *E. coli recA* required for recombination, synaptonemal complex formation, and cell cycle progression. *Cell*, **69**, 439–456.
75. Wilson,S., Tavassoli,M. and Watts,F.Z. (1998) *Schizosaccharomyces pombe* Rad32 protein: a phosphoprotein with an essential phosphoesterase motif required for repair of DNA double strand breaks. *Nucleic Acids Res.*, **26**, 5261–5269.
76. Sung,S., Li,F., Park,Y.B., Kim,J.S., Kim,A.K., Song,O.K., Kim,J., Che,J., Lee,S.E. and Cho,Y. (2014) DNA end recognition by the Mre11 nuclease dimer: insights into resection and repair of damaged DNA. *EMBO J.*, **33**, 2422–2435.
77. Ghodke,I. and Muniyappa,K. (2013) Processing of DNA double-stranded breaks and intermediates of recombination and repair by *Saccharomyces cerevisiae* Mre11 and its stimulation by Rad50, Xrs2, and Sae2 proteins. *J. Biol. Chem.*, **288**, 11273–11286.
78. Terasawa,M., Ogawa,T., Tsukamoto,Y. and Ogawa,H. (2008) Sae2p phosphorylation is crucial for cooperation with Mre11p for resection of DNA double-strand break ends during meiotic recombination in *Saccharomyces cerevisiae*. *Genes Genet. Syst.*, **83**, 209–217.
79. Manfrini,N., Guerini,I., Citterio,A., Lucchini,G. and Longhese,M.P. (2010) Processing of meiotic DNA double strand breaks requires cyclin-dependent kinase and multiple nucleases. *J. Biol. Chem.*, **285**, 11628–11637.
80. Akamatsu,Y., Murayama,Y., Yamada,T., Nakazaki,T., Tsutsui,Y., Ohta,K. and Iwasaki,H. (2008) Molecular characterization of the role of the *Schizosaccharomyces pombe nip1+/ctp1+* gene in DNA double-strand break repair in association with the Mre11-Rad50-Nbs1 complex. *Mol. Cell. Biol.*, **28**, 3639–3651.
81. Andres,S.N., Appel,C.D., Westmoreland,J.W., Williams,J.S., Nguyen,Y., Robertson,P.D., Resnick,M.A. and Williams,R.S. (2015) Tetrameric Ctp1 coordinates DNA binding and DNA bridging in DNA double-strand-break repair. *Nat. Struct. Mol. Biol.*, **22**, 158–166.
82. Williams,R.S., Dodson,G.E., Limbo,O., Yamada,Y., Williams,J.S., Guenther,G., Classen,S., Glover,J.N., Iwasaki,H., Russell,P. *et al.* (2009) Nbs1 flexibly tethers Ctp1 and Mre11-Rad50 to coordinate DNA double-strand break processing and repair. *Cell*, **139**, 87–99.
83. Lloyd,J., Chapman,J.R., Clapperton,J.A., Haire,L.F., Hartsuiker,E., Li,J., Carr,A.M., Jackson,S.P. and Smerdon,S.J. (2009) A supramodular FHA/BRCT-repeat architecture mediates Nbs1 adaptor function in response to DNA damage. *Cell*, **139**, 100–111.